Medial Temporal Lobe Contributions to Resting-State Networks

Sara Seoane
University of La Laguna https://orcid.org/0000-0002-8321-018X
Cristián Modroño
Universidad de La Laguna Facultad de Medicina
José Luis González Mora
Universidad de La Laguna Facultad de Medicina
Niels Janssen (njanssen@ull.edu.es)
Universidad de La Laguna Campus de Guajara: Universidad de La Laguna - Campus Guajara
https://orcid.org/0000-0001-9770-4458

Research Article

Keywords: Medial Temporal Lobe, Functional Connectivity, Resting-State fMRI, Independent Component Analysis, Dual Regression

Posted Date: July 8th, 2021

DOI: https://doi.org/10.21203/rs.3.rs-681614/v1

Version of Record: A version of this preprint was published at Brain Structure and Function on January 18th, 2022. See the published version at https://doi.org/10.1007/s00429-021-02442-1.

Medial temporal lobe contributions to resting-state networks

Sara Seoane[1,3,4], Cristián Modroño[2,3,4], José Luis González Mora[2,3,4] and Niels Janssen[1,3,4]

[1]Faculty of Psychology, University of La Laguna, Spain

[2]Faculty of Health Sciences, University of La Laguna, Spain

[3]Institute of Biomedical Technologies, University of La Laguna, Spain

[4]Institute of Neurosciences, University of La Laguna, Spain

Corresponding Author:

Niels Janssen

Tel: +34 922317502

e-mail: njanssen@ull.es

Abstract

The medial temporal lobe (MTL) is a set of interconnected brain regions that have been shown to play a central role in behavior as well as in neurological disease. Recent studies using resting-state functional Magnetic Resonance Imaging (rsfMRI) have attempted to understand the MTL in terms of its functional connectivity with the rest of the brain. However, the exact characterization of the whole-brain networks that co-activate with the MTL as well as how the various sub-regions of the MTL are associated with these networks remains poorly understood. Here we attempted to advance these issues by exploiting the high spatial-resolution 7T rsfMRI dataset from the Human Connectome Project with a data-driven analysis approach that relied on Independent Component Analysis (ICA) restricted to the MTL. We found that four different well-known resting-state networks co-activated with a unique configuration of MTL subcomponents. Specifically, we found that different sections of the parahippocampal cortex were involved in the default mode, visual and dorsal attention networks, sections of the hippocampus in the somatomotor and default mode networks, and the lateral entorhinal cortex in the dorsal attention network. We replicated this set of results in a validation sample. These results provide new insight into how the MTL and its subcomponents contribute to known resting-state networks. The participation of the MTL in an expanded range of resting-state networks requires a rethink of its presumed role in behavior and disease.

Keywords: Medial Temporal Lobe; Functional Connectivity; Resting-State fMRI; Independent Component Analysis; Dual Regression

Introduction

The medial temporal lobe (MTL) has received much interest in research and the clinic due to its key implication in memory processes (e.g., Alvarez & Squire, 1994; Suzuki & Amaral, 2004; Squire et al., 2007), as well as due to its involvement in several relatively common pathological conditions (e.g., temporal lobe epilepsy, schizophrenia and Alzheimer's disease; Douw et al., 2015; Seidman et al., 2003; Kenkhuis et al., 2019; Govindpani et al., 2020). The MTL encompasses a number of different anatomical structures among which figure most prominently the parahippocampal and entorhinal cortices as well as the hippocampal formation. Recent resting-state fMRI (rsfMRI) studies have attempted to understand the MTL by considering its functional connectivity with the rest of the brain (Kahn et al., 2008; Libby et al., 2012; Qin et al., 2016; Ranganath & Ritchey, 2012; Ritchey et al., 2015; Ruiz-Rizzo et al., 2020; Schröder et al., 2015; Wang et al., 2016). An on-going debate regarding this issue concerns the different whole-brain networks that connect to the MTL. Specifically, whereas the traditional view is that the MTL interacts mainly with two whole-brain networks (Kahn et al., 2008; Libby et al., 2012; Qin et al., 2016; Ranganath & Ritchey, 2012; Ritchey et al., 2015; Schröder et al., 2015; Barnett et al., 2019), other recent studies using data-driven techniques have found that the MTL connects with more than these two networks (Ruiz-Rizzo et al., 2020; Wang et al., 2016). Characterizing the whole-brain networks that co-activate with the MTL has implications for understanding its role in health and disease. One potential reason for why this issue remains unresolved may be due to the low spatial-resolution fMRI acquisition protocols used in previous studies. Here we relied on a data-driven parcellation of the MTL using the whole-brain high spatial-resolution 7T rsfMRI dataset from the Human Connectome Project (HCP).

The standard view on the connectivity between the MTL and the rest of the brain is that the MTL is connected with two distinct whole-brain networks. Both anatomical

and functional connectivity studies have shown that MTL connectivity is largely organized along a posterior-anterior gradient. For example, tract-tracing studies in monkeys and rodents have found that posterior sections of the parahippocampal cortex (PHC) and posterior sections in the hippocampal formation show increased (mono- or polysynaptic) connectivity with posterior midline regions like the retrosplenial cortex and posterior cingulate cortex, whereas anterior sections of the parahippocampal cortex and anterior sections of the hippocampal formation show increased connectivity with anterior brain regions like the orbitofrontal cortex and amygdala (Aggleton, 2012; Jones & Witter, 2007; Kobayashi & Amaral, 2007,0; Kondo et al., 2005; Rosene & Van Hoesen, 1977; Strange et al., 2014; Suzuki & Amaral, 1994). Similarly, lateral sections of the entorhinal cortex (Ent) have been associated with the posterior whole-brain network, whereas medial Ent has been associated with the anterior network (Jones & Witter, 2007; Strange et al., 2014). More recent functional connectivity studies using rsfMRI have further confirmed this bipartite organization of MTL whole-brain connectivity. Specifically, Libby et al. (2012) found that seeds placed in posterior PHC revealed co-activity with posterior midline regions like the retrosplenial cortex, precuneus, posterior cingulate and occipital cortex, whereas seeds placed in more anterior locations produced co-activity with orbitofrontal cortex and inferior temporal cortex. Other studies placing seeds in various locations along the hippocampal long-axis have revealed a similar separation of co-activity between posterior and anterior networks (Kahn et al., 2008; Qin et al., 2016), as have studies examining the entorhinal cortex (Schröder et al., 2015). In short, evidence from various sources now confirms that MTL connectivity can be associated with both a posterior and an anterior network (Ranganath & Ritchey, 2012; Ritchey et al., 2015).

However, two recent functional connectivity studies have presented results that have challenged this view. Both these studies have relied on a data-driven approach to examine functional connectivity thereby avoiding potential biases inherent in seed based

approaches (Zuo et al., 2010). Specifically, Wang et al. (2016) examined the slice-by-slice connectivity between both the parahippocampal gyrus as well as the hippocampus and the rest of the brain using a hierarchical clustering technique. Interestingly, they found that there were three connectivity clusters along the parahippocampal long axis, one in posterior PHC that connected to the aforementioned posterior network, one in anterior PHC (termed perirhinal cortex) that connected to the anterior network, and one in an even more anterior PHC location that connected to a network of regions that included the insula, post central gyrus, and amygdala. Similarly, Ruiz-Rizzo et al. (2020) examined functional connectivity of the MTL as well as the amygdala using a spatially restricted Independent Component Analysis (ICA) approach (Blessing et al., 2016; Formisano et al., 2004). They found that clusters of activity detected inside the MTL and amygdala co-activated with sets of brain regions that were interpreted in terms of five different resting-state networks. These resting-state networks were defined by the correlation of a whole-brain co-activity map with the reference networks of Allen et al. (2011). Specifically, in addition to the posterior network that correlated with the default mode network (correlation varied from $r = 0.12$ to $r = 0.48$ for different ICs), they also found that MTL was somewhat connected to other networks like the salience ($r = 0.14$), frontal ($r = 0.11$), basal ganglia ($r = 0.40$) and visual networks ($r = 0.11$).

Thus, it appears that whereas studies have found that the MTL is reliably connected to two different whole-brain networks, some studies have found it is connected to additional different whole-brain networks. One reason for the existence of this empirical discrepancy is that previous studies have relied on rather low spatial-resolution fMRI acquisition protocols ($\sim$ 3.5 mm voxels). One concern with such low resolution data is that the large size voxels may be unable to accurately separate signals from different resting-state networks leading to variability in the reported results. Here we attempted to avoid this issue by using the whole-brain high spatial-resolution rsfMRI dataset from

the HCP. This dataset has 1.6 mm isotropic resolution with whole-brain coverage and therefore increased the probability by more than 50% to better separate signals from different resting-state networks. We divided the data into test and validation datasets which were subsequently analyzed using an approach that was developed in our laboratory (Ezama et al., in press). First, we used a version of the spatially restricted group ICA technique (Blessing et al., 2016; Formisano et al., 2004) to allow for a highly sensitive detection of different sets of voxel-clusters within the MTL that are activated during the resting state at different moments in time. Next, we relied on the Dual Regression technique to obtain whole-brain functional connectivity maps (FC maps; Nickerson et al., 2017). These whole-brain FC maps therefore reflected the whole-brain co-activity with the specific MTL clusters found in the previous step. Next, the whole-brain FC maps were correlated with the 7 known resting-state networks obtained by Yeo et al. (2011) and therefore provided insight into the different resting-state networks in which the MTL participates. We then used linear mixed effect regression analyses to calculate the relative contribution of each MTL subcomponent in the different resting-state networks. Specifically, we relied on a parcellation of the MTL into anterior and posterior portions of the PHG, head, body and tail of the hippocampus and mEnt and lEnt. Finally, we replicated the FC of the MTL activation clusters with the validation dataset. These analyses therefore revealed the different whole-brain networks that co-activate with MTL as well as how the different MTL subcomponents contribute to these different whole-brain networks.

Methods

Participants

Data for all participants were downloaded from the Human Connectome Website. The initial dataset consisted of 184 participants which had participated in the 7T data acquisition. However, data from 12 participants were excluded due to presence of specific Quality Control issues identified by the HCP (i.e., QC issues A, B, C, and D). The final sample therefore consisted of 172 participants, between the ages of 22 and 35 (104 Females). Further detailed description on the study subjects may be found in Van Essen et al. (2012). The data analyses were conducted in agreement with the declaration of Helsinki and with the protocol established by the Ethics Commission for Research of the Universidad de La Laguna, the Comité de Ética de la Investigación y Bienestar Animal.

Data acquisition and preprocessing

Data packages herein used come from the WU-Minn HCP Data - 1200 Subjects data set. For this experiment, we downloaded 7T Resting State fMRI 1.6mm/32k FIX-Denoised (Compact) and Resting State fMRI FIX-Denoised (Extended) datasets. As per the HCP reference manual, these data were acquired by the Washington-University and Minnesota Consortium, with a Siemens Magnetom 7T MR Scanner and a Nova32 32-channel Siemens receive head coil from Nova Medical. Four 16-minutes-long rsfMRI acquisitions were acquired per subject. RsfMRI acquisitions alternated the direction of the phase encoding gradient, where two sessions were acquired in the posterior-to-anterior phase direction and the other two in anterior-to-posterior phase direction. For the resting-state acquisitions, participants were instructed to fix their sight on a white cross-hair over a dark background (Smith et al., 2013). MRI scanning parameters for the resting-state data were based on acquisitions of Gradient-Echo EPI volumes. Each volume contained

85 slices that were acquired with a multiband factor of 5. Slice thickness was 1.6 mm with no gap, the FOV was 208 x 208 mm, matrix size 130 x 130, resulting in 1.6 mm isotropic voxels. The TR was 1000 ms, echo time (TE) 22.2 ms, and the flip angle 45°. We used the first two of these four rsfMRI datasets as a test set (32 minutes of resting-state data), and the last two datatsets as a validation set. Both test and validation datasets had alternating phase directions.

In addition, for the structural data, we downloaded the 3T Structural Preprocessed and 3T Structural Preprocessed Extended packages. Again as per the HCP reference manual, the T1w images were acquired using a 3DMPRAGE protocol TI/TR/TE: 1000 / 2400 /2.14 ms, flip angle = 80°, resulting in 0.7 mm isotropic voxels. The T2w images were acquired using a 3D T2-SPACE protocol TR/TE: 3200/565 ms, flip angle = variable, and also resulting in 0.7 mm isotropic voxels. The structural images were acquired on a 3T Siemens Connectom Skyra scanner. The downloaded structural packages contained the T1w and T2w images for each participant as well as the full Freesurfer output and transformation matrices that were relevant for our downstream analyses (see below). For additional specific information on the pre-processing of these structural images we refer to Glasser et al. (2013).

Data Analysis

The aim of this study was to explore the different whole-brain networks that co-activate with the MTL as well as how the different MTL subcomponents contribute to these different whole-brain networks. To approach these objectives our analyses were divided into four main steps. A graphical representation of the workflow is displayed in Supplementary Figure S1.

Segmentation of MTL into subcomponents

The first step of our analysis involved the segmentation of the MTL into a number of subcomponents. This segmentation took place in a participant-specific manner, meaning that each segmentation took into account the unique shape of the MTL in each participant's brain. The MTL subcomponents were the head, body and tail of the hippocampus (hHi, bHi, and tHi), the anterior (aPHG) and posterior (pPHG) parahippocampal gyrus, as well as the medial and lateral entorhinal cortex (lEnt and mEnt). All segmentations relied on the Desikan-Killiany Atlas that is produced by Freesurfer and that was included with the downloaded dataset (i.e., the aparc+aseg atlas in Freesurfer terminology; Desikan et al., 2006). This atlas provides an automatic segmentation of the brain in terms of a set of 42 brain regions that are fitted to the unique morphology of each participant's brain. This is achieved by combining prior information about the probable spatial location of a given brain area and its surrounding structures with information about the morphology of a specific target participant brain. This way of segmenting the brain into regions is therefore more accurate than other atlas segmentations that are based on normalized brains.

To obtain the three subdivisions for the hippocampus we relied on the Hippocampal Subfields and Nuclei of the Amygdala script (v21) with the T2w image as the input (Iglesias et al., 2015). Besides segmenting the hippocampus into a set of internal subfields, this script also provides a segmentation of the hippocampus into its head, body and tail sections. In addition, anterior and posterior PHG were obtained by first extracting the parahippocampal gyrus mask from a given participant's aparc+aseg atlas. Next, in order to define aPHG and pPHG, we computed an intersection of a plane with the centroid point of the parahippocampal gyrus. The centroid point in the anterior-posterior direction was computed as the mean voxel coordinate of the parahippocampal mask along the y-axis. Consequently, the voxels posterior to that plane were defined as

pPHG and voxels anterior to the plane as aPHG. To separate the entorhinal cortex in a medial and lateral section we computed its centroid point as the mean coordinate along the x-axis and defined medial and lateral sections as above. This therefore produced participant-specific MTL subcomponent masks for head, body and tail of the hippocampus, anterior and posterior PHG, and medial and lateral entorhinal cortex (see Figure 1 for a graphical presentation of the location of the MTL and its various subcomponents for a representative participant).

Detection of MTL activation-clusters

The next step of the analysis had three goals. First, we attempted to identify those locations of the MTL that were activated during the resting-state using a data-driven approach. We first created MTL masks combining bilateral hippocampus, parahippocampal gyrus and entorhinal cortices that were specific to each participant. These masks were similar to those described above in that they were derived from the participant-specific aparc+aseg atlas, but were different because they did not distinguish between the individual MTL subcomponents. This was because we first aimed to detect locations inside the entire MTL that are active during the resting state without taking into account the various MTL subcomponents. To improve accuracy for the group analyses, each participant's MTL mask was dilated once using `fslmaths`. We then multiplied the masks with the cleaned, whole-brain resting-state fMRI data. This produced 4D fMRI files containing only the timeseries of the voxels within the MTL mask of each participant. We then performed group spatially-restricted ICA (group srICA) over these data using `melodic`(v3.15). Given the smaller sized dataset due to the masking, we used the default principal component analysis method by disabling MIGP in the melodic options (Smith et al., 2014).

One aspect of ICA is that it requires a decision about the number of dimensions under

which the analysis is performed. Here we used a method to determine the optimal number of dimensions for the ICA that was developed in our laboratory (Ezama et al., in press). Specifically, we tested across a wide range of different dimensions the relationship between a set of components found for a specific dimension and a set of known resting-state networks (Yeo et al., 2011). We then chose the dimension at which this relationship was optimal. Specifically, we first performed ICA on the same dataset at dimensions ranging from 1 to 15 in a stepwise fashion. Next, we obtained whole-brain FC maps derived from all the MTL activation clusters for each dimension. These FC maps were obtained using the Dual Regression technique (Nickerson et al., 2017). The dual regression approach consisted of a first regression on `fsl_glm` of the IC outputs of `melodic` to the cleaned and whole brain fMRI data for each participant. The output of this first step in dual regression are the time-courses of each independent component for each participant. The second step in dual regression involves a regression of the time-courses associated with each participant-specific IC map against the cleaned fMRI data. This second step produced the whole-brain maps that represent the FC between a specific IC and the rest of the brain.

These whole-brain FC maps were then correlated with the 7 resting-state networks observed by Yeo et al. (2011). This led to 15 correlation matrices of sizes $m \times n$ where m refers to the number of dimensions (1 to 15), and n to the number of resting-state networks (here 7). Inspection of these 15 correlation matrices revealed the set of resting-state networks that frequently had high correlation ($r > 0.40$) with a set of components across all dimensions. We then executed an algorithm that found a component if its maximum correlation with a given resting-state network was above a threshold ($r_{max} > 0.4$) and if this maximum correlation was sufficiently higher than the second highest correlation ($\frac{r_{max}}{r_{max2}} > 1.3$), both within the same IC and within the same resting-state network. On the assumption that a larger number of dimensions leads to more fractionated compo-

nent clusters, we then chose the smallest dimension at which this algorithm produced the largest number of ICs. This procedure therefore detected in a data-driven fashion the optimal number of dimensions for which the srICA produced the largest number of voxel-clusters inside the MTL that were both sensitive and specific to known resting-state networks.

Group-level analyses of whole-brain FC

To anticipate our results, the previous steps resulted in the detection of a set of FC maps that closely corresponded to a set of known resting-state networks. The next step in the analyses was to assess the statistical reliability of the observed whole-brain FC maps at the group level. One standard way of performing such an analysis would be to rely on a voxel-based modeling tool such as FSL randomise. However, a general problem with this approach is that it assumes that each voxel represents the exact same brain region across all participants. However, as has been discussed at length elsewhere, there is large variability in brain morphology between participants, and therefore, group level analyses of this type are sub-optimal (Anticevic et al., 2008; Fischl et al., 2008). Instead, we opted for a different analysis approach that took into account the unique morphology of each participant's brain. Specifically, we created a dataset that for each participant contained average co-activity values for all their cortical and subcortical regions from the aparc+aseg atlas. We obtained these data by intersecting each participant-specific aparc+aseg atlas with each participant-specific whole-brain FC maps obtained from Dual Regression. We then fitted these data to a linear mixed effect regression model of the form:

$$Z = hemisphere + FC\_map \times brain\_region + rand(participant), \qquad (1)$$

where *hemisphere* was a discrete co-variable with two levels (left vs right), FC_map was

a factor with number of levels equal to the number of ICs corresponding to resting-state networks detected in the previous step, $brain\_region$ was a factor with number of levels equal to the sum of the number of cortical and subcortical regions in the aparc+aseg atlas, and *participant* was a random factor with number of levels equal to the total number of participants (i.e., 172). The dependent variable was the average Z-value for each brain region computed from the participant-specific Dual Regression maps. Importantly, this mixed-effect model included a random effect term for participant that takes into account the highly probably between-participant variability that is inherent in these data. In addition, this modeling approach uses participant-specific masks that leads to group-level results that do not violate the assumption of unique brain morphology.

Within this model, our specific interest was in the interaction term of the model ($FC\_map \times brain\_region$) that provided a test of the null-hypothesis that brain regions would not have differences in mean co-activity values across the different FC maps. In other words, this interaction would not be significant if the different activation clusters detected in the MTL would be connected to the exact same whole brain resting-state networks. When this interaction was significant, we performed post-hoc tests where we compared for each FC map, the average Z-value for a given region versus the mean of the other regions (an "effect" contrast). This therefore produced for each FC map, a list of cortical and subcortical regions from the aparc+aseg atlas that had significantly more co-activity compared to all other regions.

All statistical modeling took place in the statistical computing environment `R` (v4.0.0). Mixed effect modeling relied on the `lme4` package (v1.1.23; Bates et al., 2007). Results from these regression models are presented in the form of ANOVA tables that were computed directly from the output of the mixed effect models using the `lmerTest` package (v3.1-2; Kuznetsova et al., 2017). P-values in these models were computed using the Satterthwaite correction for the degrees of freedom. Posthoc testing was performed

using the `emmeans` package (v1.4.6; Lenth et al., 2018) when a given interaction term was significant (i.e., $p < 0.05$). P-values in these posthoc tests were adjusted for multiple comparisons using the Bonferroni method. We visualized these results using the `ggseg` (v1.5.4; Mowinckel & Vidal-Piñeiro, 2019), and `ggpubr` packages (v0.3.0; Kassambara, 2018).

Relative contributions of MTL subcomponents

The previous srICA step provided us with several clusters inside the MTL that co-activated with different resting-state networks. The final step in the analyses was to determine the relative contributions of the seven MTL subcomponents (body hippocampus, anterior PHC, etc) to the different resting-state networks. To do this we intersected the participant-specific MTL subcomponent masks (described above) with each participant-specific whole-brain FC map obtained from Dual Regression. These data were then fitted to the same statistical model as described in Equation 1, except that the term $brain\_region$ now referred to the seven MTL subcomponents. As before, our specific interest was in the interaction term of the model ($FC\_map \times brain\_region$) that provided a test of the null-hypothesis of whether the seven MTL subcomponents were activated in the same way across the various FC maps. However, the post-hoc tests that were performed when this interaction term was significant differed from those described above. Specifically, in order to determine the relative contribution of the MTL subcomponents to the different resting-state networks, we first performed pairwise comparisons of all seven MTL subcomponents within each FC map. This produced a list of 21 pairwise comparisons for each FC map with a test-statistic (i.e., the z-ratio, see below) that reflected the degree to which a given component differed from another component. These pairwise test-statistics were then summed, ordered, and thresholded at > 0. This therefore produced for each detected resting-state network an ordered list of the relative

contributions of each MTL subcomponent.

Validation analysis

In order to confirm the reliability of our results, we attempted to validate our findings in a second dataset. This validation dataset consisted of two additional rsfMRI acquisitions from the same participants included in the test dataset. The two rsfMRI scans from the validation set were acquired in a different scanning session (on a different day) as the test set, but relied on the same MRI acquisition parameters. The preprocessing protocol used was the same as described for the test dataset. To validate the results, whole-brain FC maps were computed from the data in the validation set using the MTL clusters obtained in the test set. This analysis therefore provides a validation of the degree to which the MTL clusters we obtained in the spatially-restricted ICA step of the analysis generalize to different datasets. We quantified this step by computing the correlation between the whole-brain FC maps in the test and validation sets, and by comparing the correlations of the whole-brain FC maps with the reference networks of Yeo in the test and validation sets.

Results

Detection of MTL activation-clusters

The procedure for finding the optimal number of dimensions first returned that across all the 15 dimensions tested, resting-state networks 1 (visual), 2 (somatomotor), 3 (dorsal attention), and 7 (default mode) were most frequently found with correlations $r > 0.40$. In addition, the algorithm found that dimension 7 was the lowest dimension at which the largest number of ICs were strongly and uniquely connected to different resting-state networks. Specifically, we found that for dimension 7, four ICs were strongly

and uniquely correlated with four different resting-state networks: IC0 was correlated with the dorsal attention network ($r = 0.42$), IC1 was correlated with the somatomotor network ($r = 0.53$), IC2 was correlated with the default mode network ($r = 0.59$), and IC3 was correlated with the visual network ($r = 0.66$; see Table 1 for an overview of the correlations for each IC with all networks). As can be seen in Supplementary Figure S2, strong correlations ($r > 0.40$) were frequently found for these four networks in other dimensions, suggesting that the detection of these four networks was not idiosyncratic to dimension 7. In addition, as can be seen in Supplementary Figure S3, we also examined dimensions 20 and 30 and this did not lead to the detection of new networks. We can therefore conclude that for our data the specific clusters of voxels detected by the ICA using dimension 7 for IC0, IC1, IC2 and IC3 were optimal in connecting with the four known resting-state networks.

A visual presentation of the precise location of the four ICs along with their whole-brain group-level FC map derived from Dual Regression is presented in Figure 2. A further overview of all 7 ICs with their corresponding FC maps is shown Supplementary Figure S4. As can be seen in Figure 2, the four ICs are located at different positions in the MTL and revealed contrasting FC with the rest of the brain, indicating the involvement in different whole-brain networks. A more detailed view of the location of each IC within the MTL can be seen in Figure 3A and B, and C, where it can be seen that the four clusters detected by spatially restricted ICA occupy positions within the MTL that both respect and cross anatomical boundaries (e.g., IC0 seems to reflect activity in both parahippocampal gyrus as well as entorhinal cortex). The statistical reliability of the observed whole-brain networks as well as how the detected activation clusters are distributed across the various MTL subcomponents was examined in more detail below.

Group-level analyses of whole-brain FC

Group-level mixed-effect regression analysis revealed main effects of Hemisphere ($F_{1,59508} = 21.72, p < 0.0001$), IC ($F_{3,59508} = 2955.38, p < 0.0001$), and Brain Region ($F_{43,59508} = 351.21, p < 0.0001$). Most relevant for our present purposes, there was a significant interaction between IC and Brain Region ($F_{129,59508} = 589.18, p < 0.0001$), suggesting that co-activity values of brain regions differed between the various whole-brain FC maps associated with each IC. As can be seen in Table 2, post-hoc analyses revealed that IC0 and its corresponding FC map revealed regions typically associated with the dorsal-attention network like the inferior and superior parietal cortex, as well as lateral frontal areas. Similarly, as can be seen in Table 3, IC1 and its associated FC map showed regions typically associated with the somato-motor network like the amygdala and post- and pre-central gyri. In addition, as can been seen in Table 4, IC2 and its corresponding FC map revealed regions generally found in the default mode network like the isthmus cingulate (retrosplenial cortex), the precuneus, and the medial orbitofrontal cortex. Finally, as can be seen in Table 5, IC3 and its associated FC map revealed regions associated with the visual network like the cuneus and pericalcarine sulcus (see also Figures 4B, and C for a visual presentation of these results).

Relative contributions of MTL subcomponents

Multivariate regression analyses that examined the relative contribution of the MTL subcomponents to each whole-brain FC map classified as signal revealed main effects of Hemisphere ($F_{1,9432} = 45.96, p < 0.0001$), Brain Region ($F_{6,9432} = 1867.63, p < 0.0001$) and IC ($F_{3,9432} = 2378.99, p < 0.0001$). Again, important for our present purposes, the interaction between Region and IC was highly significant ($F_{18,9432} = 1442.85, p < 0.0001$), suggesting that average co-activity values for each MTL subcomponent differed between the four ICs. Further exploration of this interaction using pairwise comparisons

of the seven MTL subcomponents within each IC and then ranking the summed z-ratios revealed the relative contributions of each MTL subcomponent. Specifically, as can be seen in Table 6, summed z-ratios in IC0 (correlated with the dorsal-attention network) were strongest in pPHG, then in aPHG and finally in lEnt. Similarly, Table 6 showed that for IC1 (correlated with the somato-motor network), summed z-ratios were strongest in hHi followed by bHi, and tHi. In addition, Table 6 showed that for IC2 (correlated with the default mode network) summed z-ratios in descending order were ranked pPHG, aPHG, hHi and bHi. Finally, Table 6 showed that for IC3, summed z-ratios were strongest in pPHG (see also Figure 5 for a graphical presentation of these results).

Validation results

Calculation of the whole-brain FC maps in the validation dataset using the MTL clusters obtained from the test set described above showed highly similar results to those obtained in the test set (see Figure S5). Correlation of FC maps in the test and validation sets showed highly reliable correlations. Specifically, the FC maps associated with IC0 (DA), IC1 (SM), IC2 (DMN) and IC3 (VIS), correlated $r = 0.95, r = 0.96, r = 0.98, r = 0.97$ between the test and validation set, respectively. Finally, the pattern of correlations between the obtained FC maps in the validation set and the Yeo reference networks was highly similar (see Table S1). We therefore conclude the MTL clusters that we report are robust and generalize to different datasets.

Discussion

The aim of the current study was to characterize the different resting-state networks that co-activate with the MTL as well as detail how the different MTL subcomponents contribute to these resting-state networks. We examined this issue using the high spatial-

resolution 7T rsfMRI dataset from the HCP with a data-driven method that applied ICA in a manner that was restricted to the MTL. We found that during the resting-state, our method detected four activation clusters that were spread across the various subcomponents of the MTL. Using Dual Regression and mixed effect regression techniques, we found that these four activation clusters were functionally connected to four different whole-brain resting-state networks that relied on different contributions of MTL subcomponents. Specifically, we found that the dorsal attention network (detected with $r = 0.42$) relied primarily on the parahippocampal gyrus and entorhinal cortex, the somatomotor network ($r = 0.53$) on the hippocampus, the default mode network ($r = 0.59$) on both parahippocampal gyrus and hippocampus, and the visual network ($r = 0.66$) on the parahippocampal cortex (see Table 6 for details). These results were validated with high replication ($r > .95$) in a separate dataset.

Previous studies have reported inconsistent results on the number of whole-brain networks that co-activate with the MTL. Whereas the classical view is that the MTL is connected to a posterior and an anterior network (Kahn et al., 2008; Libby et al., 2012; Qin et al., 2016; Ranganath & Ritchey, 2012; Ritchey et al., 2015; Schröder et al., 2015), more recent studies have found that the MTL relies on additional networks beyond these two traditionally proposed (Ruiz-Rizzo et al., 2020; Wang et al., 2016). One possible reason for this empirical discrepancy is that low spatial-resolution fMRI data-acquisition protocols may hamper separability of signals and consequently produce inconsistent detection of reference networks. For example, Libby et al. (2012) used relatively low spatial-resolution fMRI and found a posterior network linked to MTL that was composed out of posterior medial temporal and parietal regions but also also included occipital cortex. In the current study we show that with high spatial-resolution fMRI there are four whole-brain resting-state networks that co-activate with the MTL (see Table 1 for details). Three of these four networks have a clear correspondence to the posterior and anterior

networks previously identified (see Tables 2-5 for anatomical details). Specifically, the default mode and visual network likely reflect the previously identified posterior network, while the somatomotor network likely reflects the anterior network. Finally, the current data further reinforce the link between the MTL and the dorsal attention network (further discussed below). Overall, the current data are in line with previous findings that have shown that more than two different whole-brain resting-state networks co-activated with the MTL (Ruiz-Rizzo et al., 2020; Wang et al., 2016).

The current results also provide insight into how the various MTL subcomponents contribute to these four resting-state networks. Specifically, the visual network relied primarily on posterior sections of the parahippocampal gyrus (PHC), and the dorsal attention network primarily on a posterior-to-anterior gradient along the parahippocampal long-axis and lateral entorhinal cortex (pPHC-aPHC-lEnt, in order of relative contribution). In addition, the default mode network relied on a more complex pattern of co-activation in both parahippocampal gyrus and hippocampus with opposite gradients in these two structures: In the parahippocampal gryus the gradient was in the posterior-anterior (pPHC-aPHC) direction, whereas in hippocampus it was in the anterior-posterior (head-body of hippocampus) direction. Finally, the somatomotor network relied primarily on the hippocampus with an anterior-posterior gradient (head-body-tail of hippocampus; see Table 6, and Figure 5 for details). These results are generally consistent with those previously observed. Specifically, the posterior network has traditionally been associated with pPHC and middle to posterior sections of the hippocampus (Kahn et al., 2008; Libby et al., 2012; Qin et al., 2016; Ranganath & Ritchey, 2012; Ritchey et al., 2015; Ruiz-Rizzo et al., 2020; Schröder et al., 2015; Wang et al., 2016). This is in line with our observations that the visual and default mode networks strongly co-activate with posterior sections of the parahippocampal gyrus and hippocampus. In addition, the anterior network is traditionally associated with anterior sections of the parahippocampal gyrus

(aPHC including perirhinal cortex) and anterior sections of the hippocampus. Interestingly, our results revealed that the somatomotor network that included areas typically associated with the anterior network like the amygdala and medial orbitofrontal cortex relied primarily on the hippocampus and not on the parahippocampal gyrus (see Table 3 and Figure 3). One possible explanation for this is that the anterior network previously observed in low spatial resolution data represented a mix between the somatomotor and dorsal attention networks thereby explaining the involvement of the aPHC. In sum, the current results therefore suggest that MTL plays a role in four different resting-state networks where these networks display distinct configurations of MTL subcomponents.

What are the implications of these data for the role of MTL in behavior and pathology? Although resting-state data cannot be used to make direct claims about function, the observation that the MTL participates in four different resting-state networks could shed light onto a more complex function of this central structure in memory and other related processes. Although the traditional view on MTL function highlights its role in memory (Squire & Zola-Morgan, 1991), there is much evidence that the MTL is also involved in perceptual and attentional processes that may contribute to performance in different memory-demanding tasks (e.g., Lawrence et al., 2020; Bussey & Saksida, 2005; Baxter, 2009). Specifically, the perirhinal cortex has been previously considered as a part of the ventral visual stream (Bussey & Saksida, 2005) and involved in the perception of objects (for a review Baxter, 2009). The hippocampus has been associated with the perception of scenes (Baxter, 2009). Furthermore, a study from Staudigl et al. (2017) found that some activity in the parahippocampal gyrus may be involved in the coordination of saccades and alpha waves for better memory encoding of visual scenes. In addition, memory problems in some pathologies may arise from disruption of the dorsal attention network (Veldsman et al., 2019), and it has been further suggested that the MTL engages in perception processes with attention as a catalyst (Ruiz et al., 2020). To

determine the precise contribution of MTL structures to different memory systems has been interpreted as a difficult task (Murray & Wise, 2004), and it may require an even harder effort to elaborate a model of MTL function given its involvement in systems not typically related to memory. These results altogether suggest that the MTL is involved in visual and somatomotor function as well as in semantic, autobiographical memory and other functions related to the default mode network (Raichle, 2015) and attention. The current results therefore highlight the importance of exploring how all these systems are affected early on in people with MTL damage, even if their deterioration is not the most noticeable at first.

Our study has several limitations. First, our conclusion that MTL relies on four particular resting-state networks is based on the specific reference atlas of Yeo et al. (2011). One concern is whether our conclusions would also hold for other reference atlases. As we show in Tables S2-S4, correlations with the 17 network atlas of Yeo et al. (2011) and the 10 networks of Smith et al. (2009) show highly similar results using these alternative atlases. Note also that correlations were much more reduced with using the Allen et al. (2011) atlas (Table S4), similar to those found by Ruiz-Rizzo et al. (2020). In addition, to perform group-level FC analysis, we used brain parcellations from the individual aparc+aseg files. The main advantage of this analysis approach is that it takes into consideration each participant's individual brain morphology, as well as that it allows for the application of more precise statistical modeling techniques. However, an obvious disadvantage is that because the activity within each brain parcel was averaged, there are limitations on the spatial precision with which an effect may be localized. We think such concerns may be further mitigated by using procedures that parcellate each aparc+aseg region to more fine grained parcels (e.g., Schaefer et al., 2018). Finally, although we compared the contributions of 7 different MTL subcomponents to whole-brain resting-state networks, we did not explicitly include the perirhinal cortex. The reason for

this is two-fold. First, the perirhinal cortex simply does not form part of the standard Desikan-Killany atlas that we used for our segmentations (Desikan et al., 2006). Second, the precise anatomical definition of perirhinal cortex remains highly disputed (Suzuki & Amaral, 1994; Augustinack et al., 2014), which complicates an accurate automatic segmentation. Thus, although the usefulness of this structure is clear (Augustinack et al., 2014; Libby et al., 2012), the integration of this structure into an automatic segmentation pipeline that also includes other MTL structures has prevented us to analyzing the contribution of this structure at this moment in time.

To conclude, the current study used a high spatial resolution dataset to examine the different whole-brain resting-state networks that co-activate with the MTL. A secondary goal was to examine how the different MTL subcomponents contribute to these resting-state networks. We found that there are four different resting-state networks that co-activate with the MTL, the default mode network, the somatomotor network, the visual network and the dorsal attention network. We found that these networks are subserved by distinct configurations of MTL subcomponent co-activity, where the default mode network relies on a combination of activity in parahippocampal gyrus and hippocampus, the somatomotor network relies on the hippocampus, the visual attention network on the parahippocampal gyrus, and the dorsal attention network on the parahippocampal gyrus and the entorhinal cortex. These results are generally in line with previous studies on this topic that have traditionally associated MTL with a set of posterior and anterior brain regions (Kahn et al., 2008; Libby et al., 2012; Qin et al., 2016; Ranganath & Ritchey, 2012; Ritchey et al., 2015; Ruiz-Rizzo et al., 2020; Schröder et al., 2015; Wang et al., 2016; Barnett et al., 2019; Vincent et al., 2006). However, our results also deviate from these previous studies and this may be the result of differences in the resolution of the fMRI acquisition protocol. Given that the MTL is traditionally associated with mnemonic functions, the involvement of the MTL in these four different networks should

motivate a rethinking of MTL function. We hope that this may produce new insights into the wide range of pathological conditions in which the MTL has been implicated.

Acknowledgements

The authors would like to thank José María Pérez González (IMETISA) for technical support. Correspondence and requests for materials should be addressed to NJ (njanssen@ull.es).

Declarations

Funding

This study was supported by grants PSI2017-84933-P and PSI2017-91955-EXP to NJ, and by TESIS2019010146 from the Board of Economy, Industry, Trade and Knowledge of the Canarian Government with a European Social Fund co-financing rate to SLS.

Conflict of interest

All authors declare that they have no conflict of interest.

Availability of data and material

Data were provided by the Human Connectome Project, WU-Minn Consortium (Principal Investigators: David Van Essen and Kamil Ugurbil; 1U54MH091657) funded by the 16 NIH Institutes and Centers that support the NIH Blueprint for Neuroscience Research; and by the McDonnell Center for Systems Neuroscience at Washington University. The data that support the findings of this study are openly available from Human Connectome Project (www.humanconnectome.org).

Code availability

Code will be made available upon reasonable request.

Ethics approval

The data analyses were conducted in agreement with the declaration of Helsinki and with the protocol established by the Ethics Commission for Research of the Universidad de La Laguna, the Comité de Ética de la Investigación y Bienestar Animal.

Consent to participate

Not applicable.

Consent for publication

Not applicable.

Abbreviations

MTL, Medial Temporal Lobe; DMN, Default Mode Network; rfMRI, resting-state functional magnetic resonance imaging; MNI, Montreal Neurological Institute 152; aPHC, anterior parahippocampal cortex; pPHC, posterior parahippocampal cortex; lEnt, lateral entorhinal cortex; mEnt, medial entorhinal cortex; hHi, head of the hippocampus; bHi, body of the hippocampus; tHi, tail of the hippocampus; Th, thalamus proper; Cd, caudate; Pu, putamen; Pal, pallidum; Hi, hippocampus; Amg, amygdala; Ac, accumbens area; vDC, ventral DC; STS, bankssts; cACC, caudal anterior cingulate; cdMF, caudal middle frontal; Cun, cuneus; Ent, entorhinal; FuG, fusiform; iP, inferior parietal; iT, inferior temporal; ICG, isthmus cingulate; lO, lateral occipital; lOF, lateral orbitofrontal; LgG, lingual gyrus; mOF, medial orbitofrontal; mT, middle temporal; PHG, parahippocampal gyrus; PCL, paracentral; IFGOp, pars opercularis; IFGOr, pars orbitalis; IFGTr, pars triangularis; PCAL, pericalcarine; PoG, postcentral; pCC, posterior cingulate; PrG, precentral; PCun, precuneus; rACg, rostral anterior cingulate; rMF,

rostral middle frontal; SF, superior frontal; SP, superior parietal; ST, superior temporal; SMG, supramarginal; FrP, frontal pole; TmP, temporal pole; TTG, transverse temporal; Ins, insula.

References

Aggleton, J. P. (2012). Multiple anatomical systems embedded within the primate medial temporal lobe: implications for hippocampal function. *Neuroscience & Biobehavioral Reviews*, *36*, 1579–1596.

Allen, E. A., Erhardt, E. B., Damaraju, E., Gruner, W., Segall, J. M., Silva, R. F., Havlicek, M., Rachakonda, S., Fries, J., Kalyanam, R. et al. (2011). A baseline for the multivariate comparison of resting-state networks. *Frontiers in systems neuroscience*, *5*, 2.

Alvarez, P., & Squire, L. R. (1994). Memory consolidation and the medial temporal lobe: a simple network model. *Proceedings of the national academy of sciences*, *91*, 7041–7045.

Anticevic, A., Dierker, D. L., Gillespie, S. K., Repovs, G., Csernansky, J. G., Van Essen, D. C., & Barch, D. M. (2008). Comparing surface-based and volume-based analyses of functional neuroimaging data in patients with schizophrenia. *Neuroimage*, *41*, 835–848.

Augustinack, J. C., Magnain, C., Reuter, M., van der Kouwe, A. J., Boas, D., & Fischl, B. (2014). Mri parcellation of ex vivo medial temporal lobe. *Neuroimage*, *93*, 252–259.

Barnett, A. J., Man, V., & McAndrews, M. P. (2019). Parcellation of the hippocampus using resting functional connectivity in temporal lobe epilepsy. *Frontiers in neurology*, *10*, 920.

Bates, D., Sarkar, D., Bates, M. D., & Matrix, L. (2007). The lme4 package. *R package version*, *2*, 74.

Baxter, M. G. (2009). Involvement of medial temporal lobe structures in memory and perception. *Neuron*, *61*, 667–677.

Blessing, E. M., Beissner, F., Schumann, A., Brünner, F., & Bär, K.-J. (2016). A data-driven approach to mapping cortical and subcortical intrinsic functional connectivity along the longitudinal hippocampal axis. *Human brain mapping*, *37*, 462–476.

Bussey, T. J., & Saksida, L. M. (2005). Object memory and perception in the medial temporal lobe: an alternative approach. *Current opinion in neurobiology*, *15*, 730–737.

Desikan, R. S., Ségonne, F., Fischl, B., Quinn, B. T., Dickerson, B. C., Blacker, D., Buckner, R. L., Dale, A. M., Maguire, R. P., Hyman, B. T. et al. (2006). An automated labeling system for subdividing the human cerebral cortex on mri scans into gyral based regions of interest. *Neuroimage*, *31*, 968–980.

Douw, L., DeSalvo, M. N., Tanaka, N., Cole, A. J., Liu, H., Reinsberger, C., & Stufflebeam, S. M. (2015). Dissociated multimodal hubs and seizures in temporal lobe epilepsy. *Annals of clinical and translational neurology*, *2*, 338–352.

Ezama, L., Hernández-Cabrera, J. A., Seoane, S., Pereda, E., & Janssen, N. (in press). Functional connectivity of the hippocampus and its subfields in resting-state networks. *European Journal Ns*, .

Fischl, B., Rajendran, N., Busa, E., Augustinack, J., Hinds, O., Yeo, B. T.,

Mohlberg, H., Amunts, K., & Zilles, K. (2008). Cortical folding patterns and predicting cytoarchitecture. *Cerebral cortex*, *18*, 1973–1980.

Formisano, E., Esposito, F., Di Salle, F., & Goebel, R. (2004). Cortex-based independent component analysis of fmri time series. *Magnetic resonance imaging*, *22*, 1493–1504.

Glasser, M. F., Sotiropoulos, S. N., Wilson, J. A., Coalson, T. S., Fischl, B., Andersson, J. L., Xu, J., Jbabdi, S., Webster, M., Polimeni, J. R. et al. (2013). The minimal preprocessing pipelines for the human connectome project. *Neuroimage*, *80*, 105–124.

Govindpani, K., Turner, C., Waldvogel, H. J., Faull, R. L., & Kwakowsky, A. (2020). Impaired expression of gaba signaling components in the alzheimer's disease middle temporal gyrus. *International Journal of Molecular Sciences*, *21*, 8704.

Iglesias, J. E., Augustinack, J. C., Nguyen, K., Player, C. M., Player, A., Wright, M., Roy, N., Frosch, M. P., McKee, A. C., Wald, L. L. et al. (2015). A computational atlas of the hippocampal formation using ex vivo, ultra-high resolution mri: application to adaptive segmentation of in vivo mri. *Neuroimage*, *115*, 117–137.

Jones, B. F., & Witter, M. P. (2007). Cingulate cortex projections to the parahippocampal region and hippocampal formation in the rat. *Hippocampus*, *17*, 957–976.

Kahn, I., Andrews-Hanna, J. R., Vincent, J. L., Snyder, A. Z., & Buckner, R. L. (2008). Distinct cortical anatomy linked to subregions of the medial temporal

lobe revealed by intrinsic functional connectivity. *Journal of neurophysiology*, *100*, 129–139.

Kassambara, A. (2018). ggpubr:"ggplot2" based publication ready plots. *R package version 0.1*, *7*.

Kenkhuis, B., Jonkman, L. E., Bulk, M., Buijs, M., Boon, B. D., Bouwman, F. H., Geurts, J. J., van de Berg, W. D., & van der Weerd, L. (2019). 7t mri allows detection of disturbed cortical lamination of the medial temporal lobe in patients with alzheimer's disease. *NeuroImage: Clinical*, *21*, 101665.

Kobayashi, Y., & Amaral, D. G. (2003). Macaque monkey retrosplenial cortex: Ii. cortical afferents. *Journal of Comparative Neurology*, *466*, 48–79.

Kobayashi, Y., & Amaral, D. G. (2007). Macaque monkey retrosplenial cortex: Iii. cortical efferents. *Journal of Comparative Neurology*, *502*, 810–833.

Kondo, H., Saleem, K. S., & Price, J. L. (2005). Differential connections of the perirhinal and parahippocampal cortex with the orbital and medial prefrontal networks in macaque monkeys. *Journal of Comparative Neurology*, *493*, 479–509.

Kuznetsova, A., Brockhoff, P. B., Christensen, R. H. et al. (2017). lmertest package: tests in linear mixed effects models. *Journal of statistical software*, *82*, 1–26.

Lawrence, A. V., Cardoza, J., & Ryan, L. (2020). Medial temporal lobe regions mediate complex visual discriminations for both objects and scenes: A process-based view. *Hippocampus*, .

Lenth, R., Singmann, H., Love, J., Buerkner, P., & Herve, M. (2018). Emmeans: Estimated marginal means, aka least-squares means. *R package version*, *1*, 3.

Libby, L. A., Ekstrom, A. D., Ragland, J. D., & Ranganath, C. (2012). Differential connectivity of perirhinal and parahippocampal cortices within human hippocampal subregions revealed by high-resolution functional imaging. *Journal of Neuroscience*, *32*, 6550–6560.

Mowinckel, A. M., & Vidal-Piñeiro, D. (2019). Visualisation of brain statistics with r-packages ggseg and ggseg3d. *arXiv preprint arXiv:1912.08200*, .

Murray, E. A., & Wise, S. P. (2004). What, if anything, is the medial temporal lobe, and how can the amygdala be part of it if there is no such thing? *Neurobiology of learning and memory*, *82*, 178–198.

Nickerson, L. D., Smith, S. M., Öngür, D., & Beckmann, C. F. (2017). Using dual regression to investigate network shape and amplitude in functional connectivity analyses. *Frontiers in neuroscience*, *11*, 115.

Qin, S., Duan, X., Supekar, K., Chen, H., Chen, T., & Menon, V. (2016). Large-scale intrinsic functional network organization along the long axis of the human medial temporal lobe. *Brain Structure and Function*, *221*, 3237–3258.

Raichle, M. E. (2015). The brain's default mode network. *Annual review of neuroscience*, *38*, 433–447.

Ranganath, C., & Ritchey, M. (2012). Two cortical systems for memory-guided behaviour. *Nature Reviews Neuroscience*, *13*, 713–726.

Ritchey, M., Libby, L. A., & Ranganath, C. (2015). Cortico-hippocampal systems involved in memory and cognition: the pmat framework. In *Progress in brain research* (pp. 45–64). Elsevier volume 219.

Rosene, D. L., & Van Hoesen, G. W. (1977). Hippocampal efferents reach widespread areas of cerebral cortex and amygdala in the rhesus monkey. *Science*, *198*, 315–317.

Ruiz, N. A., Meager, M. R., Agarwal, S., & Aly, M. (2020). The medial temporal lobe is critical for spatial relational perception. *Journal of Cognitive Neuroscience*, (pp. 1–16).

Ruiz-Rizzo, A. L., Beissner, F., Finke, K., Müller, H. J., Zimmer, C., Pasquini, L., & Sorg, C. (2020). Human subsystems of medial temporal lobes extend locally to amygdala nuclei and globally to an allostatic-interoceptive system. *NeuroImage*, *207*, 116404.

Schaefer, A., Kong, R., Gordon, E. M., Laumann, T. O., Zuo, X.-N., Holmes, A. J., Eickhoff, S. B., & Yeo, B. T. (2018). Local-global parcellation of the human cerebral cortex from intrinsic functional connectivity mri. *Cerebral cortex*, *28*, 3095–3114.

Schröder, T. N., Haak, K. V., Jimenez, N. I. Z., Beckmann, C. F., & Doeller, C. F. (2015). Functional topography of the human entorhinal cortex. *Elife*, *4*, e06738.

Seidman, L. J., Pantelis, C., Keshavan, M. S., Faraone, S. V., Goldstein, J. M., Horton, N. J., Makris, N., Peter, F., Caviness, V. S., & Tsuang, M. T. (2003). A review and new report of medial temporal lobe dysfunction as a vulnerability

indicator for schizophrenia: a magnetic resonance imaging morphometric family study of the parahippocampal gyrus. *Schizophrenia bulletin*, *29*, 803–830.

Smith, S. M., Beckmann, C. F., Andersson, J., Auerbach, E. J., Bijsterbosch, J., Douaud, G., Duff, E., Feinberg, D. A., Griffanti, L., Harms, M. P. et al. (2013). Resting-state fmri in the human connectome project. *Neuroimage*, *80*, 144–168.

Smith, S. M., Fox, P. T., Miller, K. L., Glahn, D. C., Fox, P. M., Mackay, C. E., Filippini, N., Watkins, K. E., Toro, R., Laird, A. R. et al. (2009). Correspondence of the brain's functional architecture during activation and rest. *Proceedings of the national academy of sciences*, *106*, 13040–13045.

Smith, S. M., Hyvärinen, A., Varoquaux, G., Miller, K. L., & Beckmann, C. F. (2014). Group-pca for very large fmri datasets. *Neuroimage*, *101*, 738–749.

Squire, L. R., Wixted, J. T., & Clark, R. E. (2007). Recognition memory and the medial temporal lobe: a new perspective. *Nature Reviews Neuroscience*, *8*, 872–883.

Squire, L. R., & Zola-Morgan, S. (1991). The medial temporal lobe memory system. *Science*, *253*, 1380–1386.

Staudigl, T., Hartl, E., Noachtar, S., Doeller, C. F., & Jensen, O. (2017). Saccades are phase-locked to alpha oscillations in the occipital and medial temporal lobe during successful memory encoding. *PLoS biology*, *15*, e2003404.

Strange, B. A., Witter, M. P., Lein, E. S., & Moser, E. I. (2014). Functional organization of the hippocampal longitudinal axis. *Nature Reviews Neuroscience*, *15*, 655–669.

Suzuki, W. A., & Amaral, D. G. (2004). Functional neuroanatomy of the medial temporal lobe memory system. *Cortex: A Journal Devoted to the Study of the Nervous System and Behavior*, .

Suzuki, W. L., & Amaral, D. G. (1994). Perirhinal and parahippocampal cortices of the macaque monkey: cortical afferents. *Journal of comparative neurology*, *350*, 497–533.

Van Essen, D. C., Ugurbil, K., Auerbach, E., Barch, D., Behrens, T., Bucholz, R., Chang, A., Chen, L., Corbetta, M., Curtiss, S. W. et al. (2012). The human connectome project: a data acquisition perspective. *Neuroimage*, *62*, 2222–2231.

Veldsman, M., Zamboni, G., Butler, C., & Ahmed, S. (2019). Attention network dysfunction underlies memory impairment in posterior cortical atrophy. *NeuroImage: Clinical*, *22*, 101773.

Vincent, J. L., Snyder, A. Z., Fox, M. D., Shannon, B. J., Andrews, J. R., Raichle, M. E., & Buckner, R. L. (2006). Coherent spontaneous activity identifies a hippocampal-parietal memory network. *Journal of neurophysiology*, *96*, 3517–3531.

Wang, S.-F., Ritchey, M., Libby, L. A., & Ranganath, C. (2016). Functional connectivity based parcellation of the human medial temporal lobe. *Neurobiology of Learning and Memory*, *134*, 123–134.

Yeo, B. T., Krienen, F. M., Sepulcre, J., Sabuncu, M. R., Lashkari, D., Hollinshead, M., Roffman, J. L., Smoller, J. W., Zöllei, L., Polimeni, J. R. et al. (2011). The organization of the human cerebral cortex estimated by intrinsic functional connectivity. *Journal of neurophysiology*, .

Zuo, X.-N., Kelly, C., Adelstein, J. S., Klein, D. F., Castellanos, F. X., & Milham, M. P. (2010). Reliable intrinsic connectivity networks: test–retest evaluation using ica and dual regression approach. *Neuroimage*, *49*, 2163–2177.

Tables

Table 1: Table of correlations of the FC maps with resting-state networks.

Yeo et al. (2011), 7 networks	IC0	IC1	IC2	IC3
Visual	0.13	0.12	0.02	0.66
Somatomotor	0.02	0.53	0.03	0.24
Dorsal Attention	0.42	0.05	0.01	0.16
Ventral Attention & Salience	0.03	0.01	0.02	0.21
Limbic	0.04	0.10	0.00	0.02
Executive Control	0.20	0.02	0.11	0.00
Default Mode	0.12	0.20	0.59	0.01

Table 2: Cortical and subcortical areas showing reliable co-activity with IC0 (correlated with Dorsal Attention network) relative to the mean co-activity value of all other areas. p-values corrected for multiple comparisons using Bonferroni correction.

region	z.ratio	p.value
parahippocampal	47.72	0.000E+00
inferior parietal	40.13	0.000E+00
precuneus	24.03	5.577E-126
fusiform	20.59	1.569E-92
caudal middle frontal	17.42	2.406E-66
inferior temporal	16.61	2.535E-60
isthmus cingulate	11.68	7.301E-30
superior parietal	9.17	2.068E-18
supramarginal	8.38	2.194E-15
entorhinal	7.79	2.789E-13
middle temporal	5.78	3.301E-07
medial orbitofrontal	4.10	1.802E-03

Table 3: Cortical and subcortical areas showing reliable co-activity with IC1 (correlated with Somatomotor network) relative to the mean co-activity value of all other areas. p-values corrected for multiple comparisons using Bonferroni correction.

region	z.ratio	p.value
amygdala	55.30	0.000E+00
hippocampus	53.71	0.000E+00
postcentral	49.85	0.000E+00
paracentral	34.58	2.413E-260
superior temporal	27.76	5.009E-168
precentral	21.26	1.237E-98
bankssts	19.23	8.143E-81
medial orbitofrontal	13.27	1.406E-38
entorhinal	12.17	1.874E-32
fusiform	11.51	5.215E-29
temporal pole	10.15	1.421E-22
cuneus	10.00	6.511E-22
frontal pole	8.82	4.865E-17
isthmus cingulate	7.39	6.378E-12
middle temporal	7.19	2.866E-11
transverse temporal	3.83	5.402E-03
parahippocampal	3.62	1.279E-02

Table 4: Cortical and subcortical areas showing reliable co-activity with IC2 (correlated with Default Mode network) relative to the mean co-activity value of all other areas. p-values corrected for multiple comparisons using Bonferroni correction.

region	z.ratio	p.value
isthmus cingulate	70.52	0.000E+00
precuneus	50.65	0.000E+00
parahippocampal	34.93	1.301E-265
inferior parietal	32.82	1.256E-234
rostral anterior cingulate	32.67	1.781E-232
frontal pole	26.58	5.334E-154
medial orbitofrontal	26.31	7.064E-151
caudal middle frontal	21.98	1.828E-105
superior frontal	18.42	3.889E-74
middle temporal	13.09	1.656E-37
hippocampus	11.37	2.489E-28
posterior cingulate	8.69	1.499E-16
caudate	7.09	5.923E-11
ventral DC	6.21	2.345E-08
temporal pole	4.91	3.874E-05
rostral middle frontal	4.19	1.188E-03
brain stem	3.53	1.777E-02

Table 5: Cortical and subcortical areas showing reliable co-activity with IC3 (correlated with Visual network) relative to the mean co-activity value of all other areas. p-values corrected for multiple comparisons using Bonferroni correction.

region	z.ratio	p.value
cuneus	99.93	0.000E+00
pericalcarine	89.54	0.000E+00
lingual	77.22	0.000E+00
superior parietal	40.98	0.000E+00
precuneus	23.29	2.205E-118
parahippocampal	18.32	2.276E-73
fusiform	16.28	5.737E-58
lateral occipital	15.69	7.799E-54
postcentral	11.46	9.415E-29
paracentral	8.86	3.329E-17
caudal anterior cingulate	7.90	1.164E-13
transverse temporal	6.98	1.274E-10
precentral	4.16	1.375E-03

Table 6: Strongest contrast for MTL substructures for each IC. Contrast based on the sum of pairwise z-ratio differences for all substructures. Rank indicates the order of the substructures relative contribution for each IC.

Region	IC	summed z-ratio	rank	network
pPHG	0	366.37	1	
aPHG	0	158.15	2	Dorsal Attention
lEnt	0	8.44	3	
hHi	1	342.85	1	
bHi	1	180.64	2	Somatomotor
tHi	1	141.79	3	
pPHG	2	233.97	1	
aPHG	2	122.92	2	Default Mode
hHi	2	30.40	3	
bHi	2	10.85	4	
pPHG	3	456.13	1	Visual

Figures

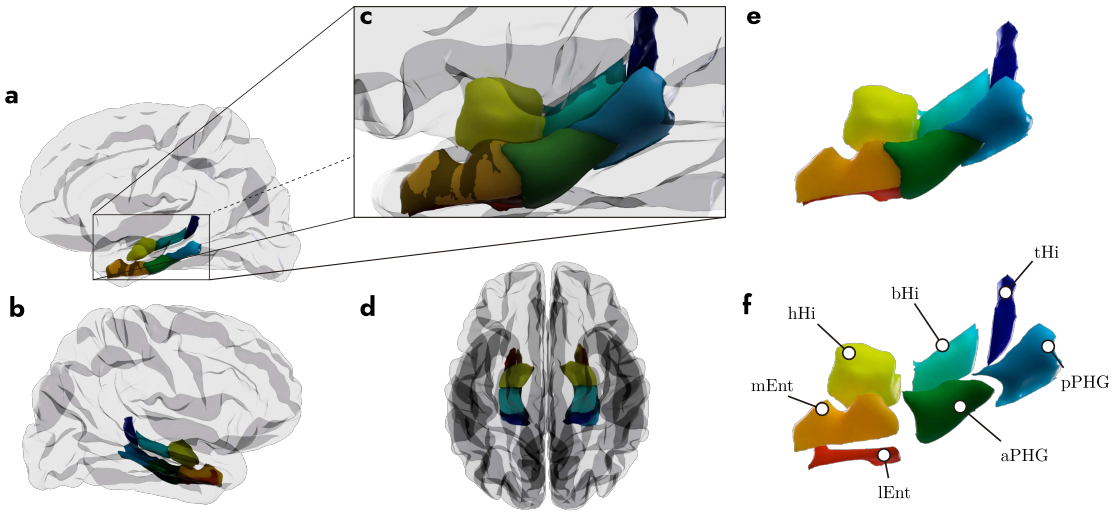

Figure 1: Visualization of the MTL subcomponents. Location of MTL in the left (a) and right hemispheres (b) of the whole-brain along with a zoomed view (c) as well as a dorsal view (d). Panels E and F highlight the various substructures that make up the MTL, posterior parahippocampal gyrus (pPHG), anterior parahippocampal gyrus (aPHG), hippocampal tail (tHi), body (bHi) and head (hHi), as well as medial (mEnt) and lateral (lEnt) entorhinal cortex.

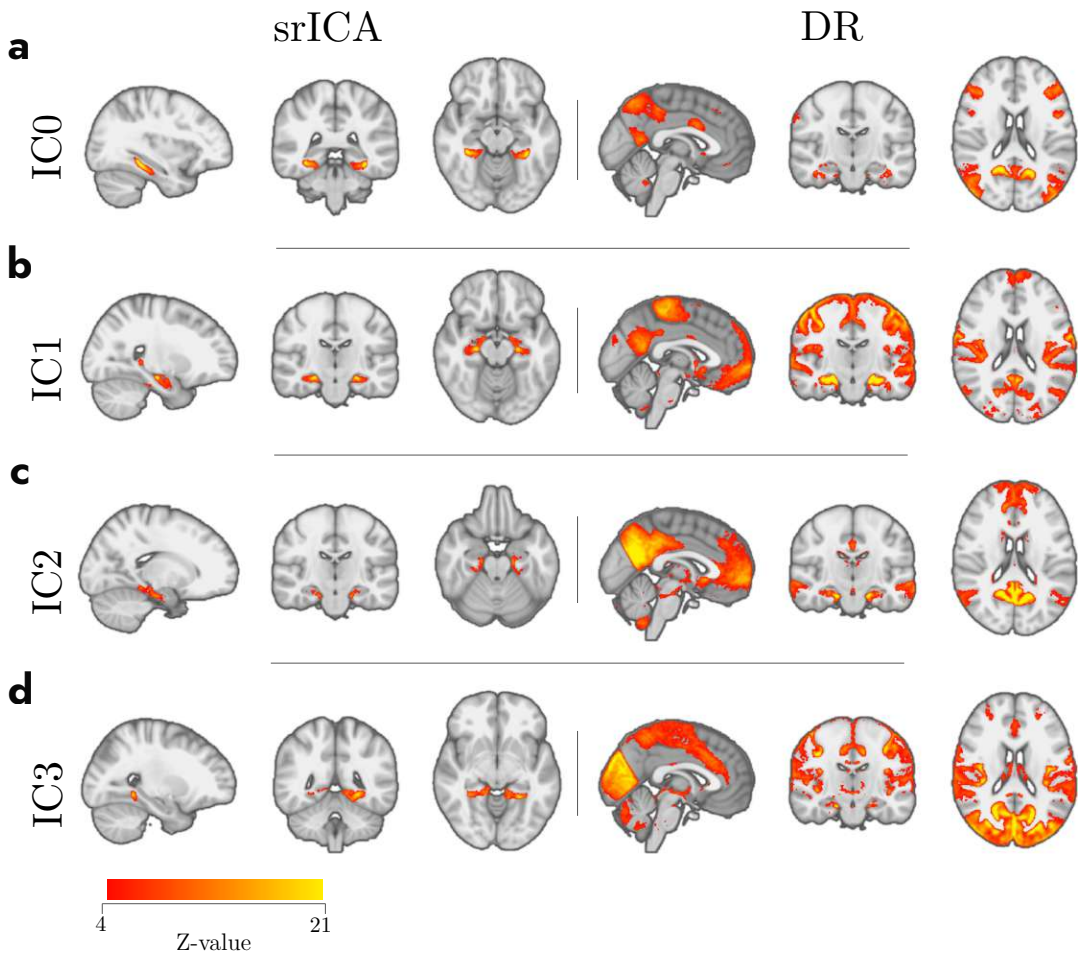

Figure 2: The subset of Independent Components (IC0, a; IC1, b; IC2, c; IC3, d) detected as signal from the spatially restricted ICA (srICA, left column), and their corresponding whole-brain functional connectivity maps derived from Dual Regression (DR, right column). The color gradient represents the group level of co-activation quantified in Z-values. Note how different IC hotspots inside the MTL connect to different areas of the brain. srICA, spatially restricted Independent Component Analysis; IC, Independent Component; DR, Dual Regression.

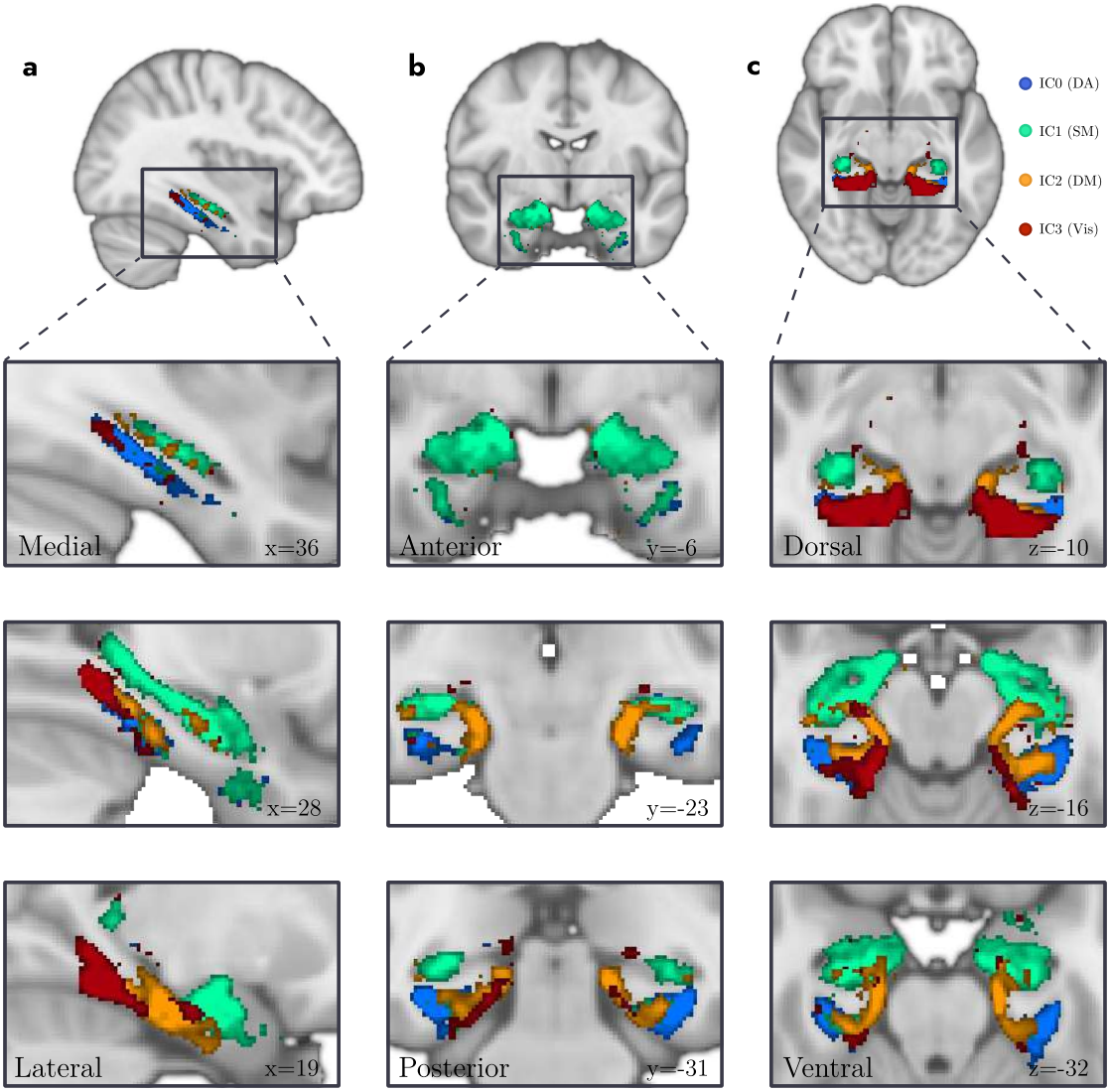

Figure 3: Detailed location of the main target hotspots in the MTL detected with spatially restricted ICA. IC0 (blue), IC1 (green), IC2 (orange) and IC3 (red) in saggital (a) and coronal (b), and axial (c) views. Note how ICs both respect and cross anatomical boundaries suggesting inter-structure communication. Slices in 1 mm MNI152 space. DA, dorsal attention; SM, somatomotor; DM, default mode; Vis, visual.

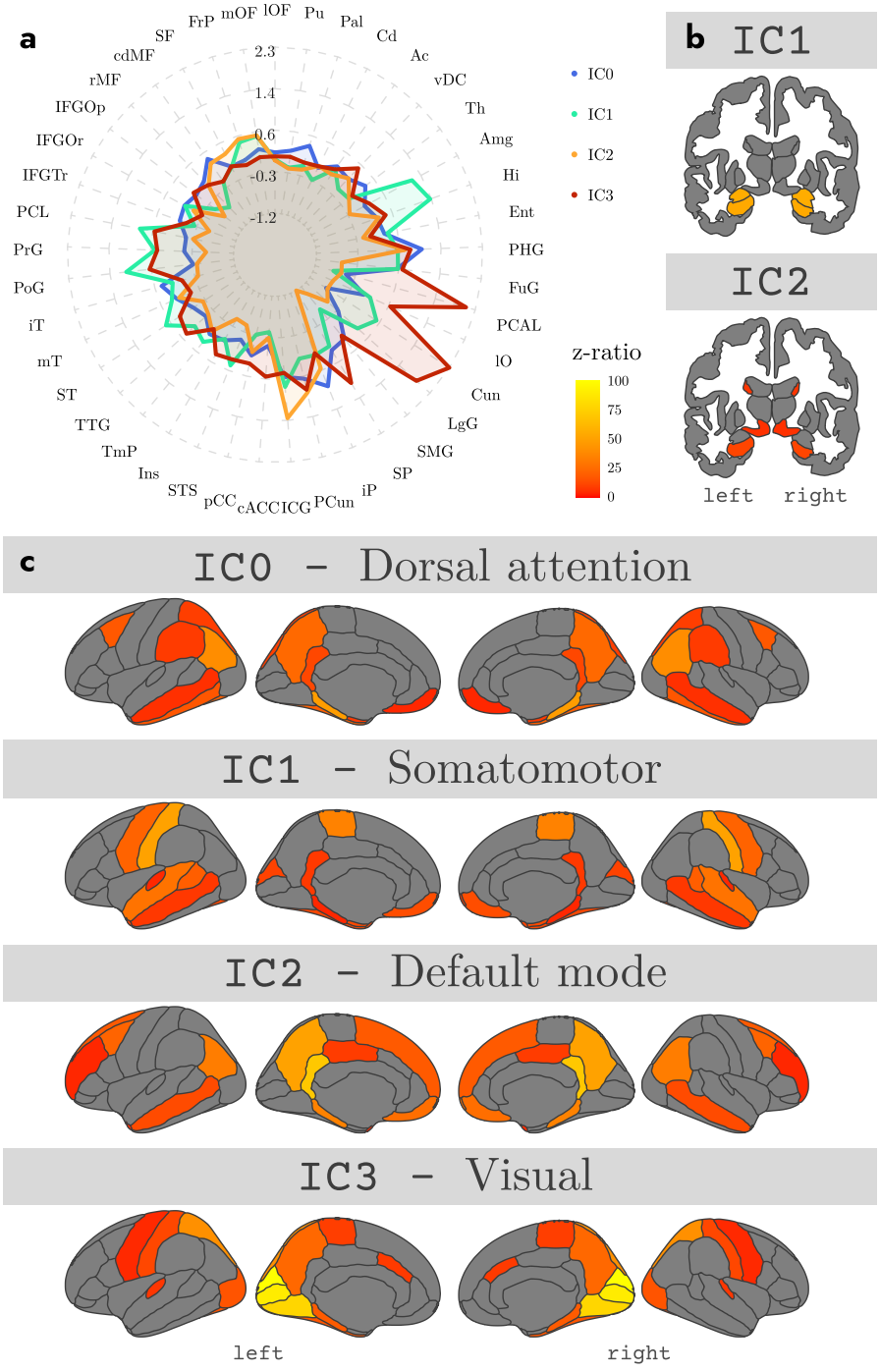

Figure 4: Spiderplot representation of functional connectivity (estimated marginal coefficients) between the four IC hotspots (IC0, IC1, IC2, IC3) and the rest of the brain (a), as well as functional connectivity results from group-based analyses in subcortical (b) and cortical (c) regions for each of the different ICs (see Tables 2-5 for details).

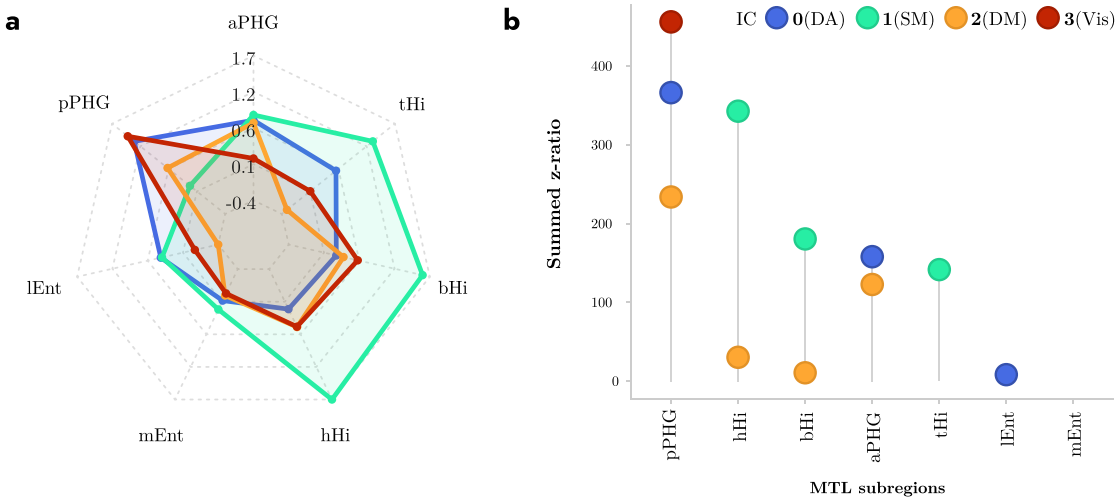

Figure 5: Spiderplot representation of co-activity values (estimated marginal coefficients) within the 7 MTL regions for each of the four ICs (a), as well as the relative contribution (in terms of summed z-values) from each MTL region to each of the four ICs (b). Note that, for example, IC0 (Dorsal Attention, blue dots) relies on contributions from pPHG and aPHG and lateral Ent, and that IC2 (Default Mode, green dots) relied primarily on pPHG, aPHG, and on head and body of the hippocampus. DA, dorsal attention; SM, somatomotor; DM, default mode; Vis, visual.

Supplementary Files

This is a list of supplementary files associated with this preprint. Click to download.

- MTLFCpaperSupplementaryInformation.pdf